CO2 capture from syngas by an adsorption process at a biomass gasification CHP plant: Its comparison with amine-based CO2 capture

International Journal of Greenhouse Gas Control 35 (2015) 71–81

Contents lists available at ScienceDirect

International Journal of Greenhouse Gas Control

journal homepage: www.elsevier.com/locate/ijggc

CO_2 capture from syngas by an adsorption process at a biomass gasification CHP plant: Its comparison with amine-based CO_2 capture

Gabriel David Oreggioni, Stefano Brandani, Mauro Luberti, Yusuf Baykan, Daniel Friedrich, Hyungwoong Ahn*

Scottish Carbon Capture and Storage Centre, Institute for Materials and Processes, School of Engineering, The University of Edinburgh, Mayfield Road, Edinburgh EH9 3JL, UK

ARTICLE INFO

Article history:
Received 25 November 2014
Received in revised form 13 January 2015
Accepted 16 January 2015

Keywords:
Biomass gasification CHP plant
Carbon capture
Pressure Vacuum Swing Adsorption process
Amine process
Process simulation

ABSTRACT

An exemplary 10 MW_{th} biomass-fuelled CHP plant equipped with a FICFB (Fast Internally Circulating Fluidised Bed) gasifier and a Jenbacher type 6 gas engine was simulated using Honeywell UniSim R400 to estimate the power and thermal outputs. The biomass gasification CHP plant was integrated with either a pre-combustion adsorptive capture process or a conventional post-combustion amine process to achieve carbon-negative power and heat generation. The practical maximum of carbon capture rate achievable with an adsorptive CO_2 capture process applied to a syngas stream was 49% in overall while the amine process could boost the carbon capture rate up to 59%. However, it was found that the two-stage, two-bed PVSA (Pressure Vacuum Swing Adsorption) unit would have a clear advantage over the conventional amine processes in that the CHP plant integrated with the PVSA unit could achieve 1.7% points higher net electrical efficiency and 12.8% points higher net thermal efficiency than the CHP plant integrated with the amine process.

1. Introduction

Different technologies and processes are under consideration to reduce CO_2 emissions originating from combustion aiming to reverse the increase of the atmospheric CO_2 concentration that could lead to a harmful climate change (IPCC, 2005). The latest revisions of the IPCC report (IPCC, 2014) highlighted application of carbon capture and storage to biomass-fuelled CHP plants as a promising option for negative emission energy generation.

Currently there are two commercial processes deemed most conventional for producing heat and power from biomass with sufficiently high efficiencies, such as (1) direct combustion of biomass combined with a back-pressure steam turbine and subsequent heat recovery and (2) biomass gasification for generating a synthesis gas that fuels a gas engine for power generation in combination with heat recovery. In particular, CHP plants driven by biomass gasification which are capable of achieving much higher power efficiency would be preferred to those by direct combustion for their applications where higher power-to-heat output ratios are required (Bridgewater, 1995; US EPA, 2007; Obernberger and Thek, 2008; Francois et al., 2013; Sartor et al., 2014).

Biomass-fuelled CHP plants are naturally carbon-neutral so there is not any net CO_2 addition to atmosphere as a result of running biomass-fuelled CHP plants if the CO_2 emissions involved in biomass transport and processing are neglected. If a carbon capture unit is integrated with the biomass-fuelled CHP plant, it is expected to achieve carbon-negative energy generation in overall due to some CO_2 in the air being consumed in the process of growing biomass through photosynthesis.

When the biomass gasification CHP plant is considered as a base case, it is conceivable to apply a carbon capture process to two different gas streams on the CHP plant. One is a gas stream combining the two flue gas streams originating from the gasifier combustion reactor and the gas engine. And the other is the synthesis gas (syngas) stream generated by biomass gasification.

It is well known that carbon capture from flue gas can be performed effectively by amine processes (Ahn et al., 2013). However, as the syngas stream has a significantly lower volumetric flowrate, approximately 11% of the flue gas, and a higher CO_2 mole fraction of 33 vol.% in comparison to 13 vol.% in the flue gas, the optimal gas separation technology may not be necessarily the amine process. In particular for the 10 MW_{th} scale biomass CHP plant of this study the syngas flowrate of around 0.8 m^3/s is so

* Corresponding author. Tel.: +44 0 1316505891.
E-mail address: H.Ahn@ed.ac.uk (H. Ahn).

http://dx.doi.org/10.1016/j.ijggc.2015.01.008
1750-5836/

Nomenclature

F	molar flowrate (mol/s)
P	power (MW_e or kW_e)
P_{des}	desorption pressure (bar)
H	heat (MW_{th})
Q	heat input by feed biomass (MW_{th})
M	molecular weight (kg/mol)

Greek letters

ρ	gas density (kg/m^3)
γ	ratio of specific heats (C_p/C_v)
η_e	net electrical efficiency (−)
η_{th}	net thermal efficiency(−)
η_{Blower}	blower efficiency (−)
$\eta_{Vacuum\ pump}$	vacuum pump efficiency (−)

Subscript

c	consumption
g	generation
gasification	gasification section of a biomass gasification CHP plant
engine	gas engine section of a biomass gasification CHP plant

low that an adsorption process can be considered as an alternative to conventional absorption-based separation processes for this small- to medium- scale application (Yang, 1997; Ruthven, 1984).

The adsorptive capture process applied to the syngas can be designed to achieve over 95% CO_2 purity and in the vicinity of 90% carbon recovery from the syngas before fuel gas combustion. At the same time, the loss of valuable H_2 to the CO_2 product can be minimized by selecting an adsorbent having an extremely high selectivity of CO_2 over H_2. Since the pressures of both syngas and flue gas are close to atmospheric pressure, the adsorptive carbon capture design must be a Pressure Vacuum Swing Adsorption (PVSA) system that has been developed for a post-combustion capture process (Xiao et al., 2008; Shen et al., 2012; Wang et al., 2013; Krishnamurthy et al., 2014). They have reported the total power consumption of around 0.5 to 0.8 MJ_e/kg CO_2 with well-designed adsorption processes using either a one-stage, multiple-column system or a two-stage, two-column system. In comparison, a conventional monoethanolamine (MEA) capture plant applied to the same flue gas spends 3.5 MJ_{th}/kg CO_2 for the reboiler duty and 0.05 MJ_e/kg CO_2 for pumps and blowers (Ahn et al., 2013). By converting the heat duty to its equivalent power, the total power consumption of a MEA capture unit amounts to 1.1 MJ_e/kg CO_2 that appears to be greater than those of adsorptive capture units. However a simple comparison of the two figures, which may lead to an impetuous conclusion of adsorptive capture processes being superior to amine capture processes, should not be made. This is because the energy penalties did not include (1) power loss caused by the shift reaction preceding the adsorptive capture unit for enriching CO_2 in the syngas and (2) energy consumption required for CO_2 compression starting from two different pressures of CO_2 products. Since the adsorption process spends only power but the amine process needs mostly heat, the energy penalties of the two processes have usually been compared on the basis of the specific power consumption per unit CO_2 captured as shown above for PC-fired boiler power plants (Ahn et al., 2013). However, it is not trivial to convert thermal consumption to its equivalent power consumption in case of biomass gasification CHP plants since there is no steam cycle available for the CHP plant. In other words, in case of PC-fired boiler power plants, the LP steam required for operating the stripper reboiler can be sourced from the existing steam cycle by steam extraction which is directly relating to energy penalty. However, in case of a biomass gasification CHP plant, the LP steam for the stripper reboiler that must be generated additionally cannot be converted to its equivalent power consumption since there is no steam turbine in the plant. Therefore, the factor for converting the reboiler duty to its equivalent power that was devised for amine capture processes in case of a PC-fired boiler power plant cannot be directly utilised for a biomass gasification CHP plant. Due to these issues being raised we decided to simulate the entire biomass gasification CHP plant integrated with a carbon capture process in order to quantify reduction of the overall net power and thermal efficiencies and subsequently estimate the specific energy penalty in the context of the overall process performance.

In this study, it was trialed to construct a detailed process flowsheet for a biomass gasification CHP plant as a base case in the first place. Then the base case plant was integrated with two different carbon capture processes: a two-stage, two-column PVSA system (case 1) and a conventional MEA carbon capture process (case 2) for comparing the energy penalties involved in the two carbon capture processes. The key stream information estimated by simulating the base case and two carbon capture cases are reported in Appendix A. Supplementary data along with simplified process schematics.

2. Base case: A biomass gasification CHP plant with a gas engine

A biomass gasification CHP plant with a gas engine selected as a base case was simulated in reference to the existing plant in operation (Simader, 2004). In this process, the biomass feed is converted into a syngas by a Fast Internally Circulating Fluidized Bed (FICFB) process and then the syngas is fed to a gas engine (GE Jenbacher Type 6) for power generation. In addition to power, heat can also be generated by recovering heat from both gasifier and gas engine. In this study, the process was designed on a basis of around 10 MW_{th} thermal input of biomass feed. The process flowsheet is presented in Fig. 1.

2.1. FICFB gasifier

The FICFB gasification process is composed of two reaction zones: gasification and combustion zones (Hofbauer et al., 1997). The biomass feed (beech chips) is composed of 48.26% carbon, 5.82% hydrogen, 45.67% oxygen, 0.22% nitrogen and 0.03% sulphur in weight on the moisture ash-free basis (maf) and its proximate analysis and heating value were also reported in their work (Schuster et al., 2001). The wet biomass feed containing 25 wt% H_2O is gasified by steam generated on the spot and heat carried by hot inert material heated at the combustion zone. Approximate 15% of the total carbon contained in the biomass feed is not gasified but deposited on the circulating inert material (Schuster et al., 2001). In order to simulate it, a component separator was used to remove 15% of the carbon in the biomass feed in prior to the biomass feed being sent to the gasification zone. The gasification zone as well as the combustion zone was simulated using a Gibbs reactor. The syngas composition estimated in this simulation was 46.4% H_2, 26.2% CO, 16.4% H_2O, 10.1% CO_2, 0.1% CH_4 and 0.8% N_2 in molar percentage that was very close to those of the reference study (Schuster et al., 2001).

The syngas generated at the gasification reactor is cleaned by a scrubber and then it is split into two streams. One syngas stream, together with the unconverted carbon deposit, is sent to the combustion zone as a fuel for heating the circulating inert material while the other is directly fed to a gas engine. The carbon deposit on the inert material and the part of syngas being recycled are both

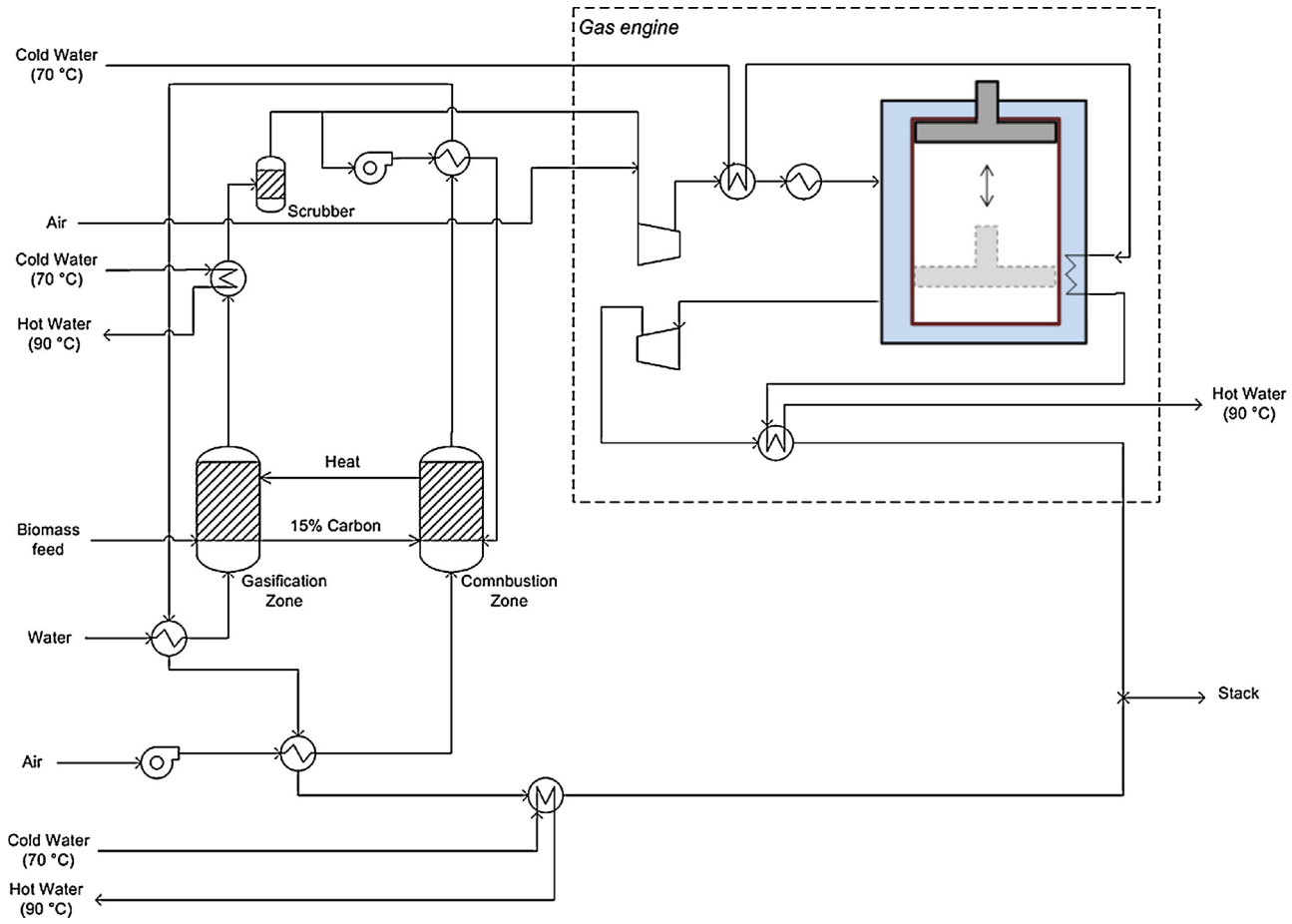

Fig. 1. Schematic diagram of a biomass gasification CHP plant equipped with a FICFB gasifier and a turbocharged gas engine (Base case).

combusted with air in the combustion zone to heat up the inert material to an extent that they can provide sufficient heat for gasifying the biomass feed at the gasification zone. The thermal energy of two hot streams leaving the gasification and combustion zones are recovered by generating gasification steam, preheating air and syngas, as well as producing hot water.

2.2. Gas engine

The Jenbacher Type 6 gas engine, currently one of the most advanced gas engines, was chosen for generating power by combusting the fuel gas generated by the FICFB biomass gasifier with air since it can serve power generation in the range of 1.5 to 4.4 MW with very high electrical efficiency ranging from 41% to 45% (GE Energy, 2009). Among several Jenbacher Type 6 models, J620 was chosen for this study since the electricity capacity (3.1 MW_e) is close to those designed in this study (GE Energy, 2010a). The gas engine was simulated using UniSim to find out operating conditions of various units and streams constituting the gas engine. Constructing a reliable simulator for this gas engine is essential for estimating the power and thermal outputs of a gas engine running with different feed gases. In case of the biomass gasification CHP plant being integrated with an adsorptive capture process, the gas engine runs with a syngas stream of which the composition is very different from that in the base case since the syngas is enriched with CO_2 by shift reactors and subsequently decarbonised by an adsorptive CO_2 capture unit. The single-stage turbocharged Otto cycle of the J620 gas engine was configured in reference to GE Energy (2010b) as shown in Fig. 1. First, all the operating conditions of the four steps of the Otto cycle, a compressor and a turbine as well as heat exchangers and coolers were determined such that they could reproduce the electrical and thermal efficiencies reported by the vendor in case of a natural gas feed having the methane number of 70 (GE Energy, 2009). The gas engine simulation must meet the following design parameters presented by the technical datasheet (GE Energy, 2009).

- The mean efficiency pressure is around 20 bar for a feed having the methane number of 70.
- The compression ratio is 11, implying that the pressure of a gas at the end of the compression step can vary with the gas composition to achieve the same compression ratio.
- The exhaust gas outlet temperature = 120 °C for natural gas, 180 °C for biogas.
- Hot water temperatures at inlet and outlet = 70/90 °C.

In simulating the gas engine with the natural gas feed (methane number = 70), it was tried to set up the gas engine simulation so that the electrical and thermal outputs could be as close to those in the reference (GE Energy, 2009) as possible with the above-mentioned design parameters met at the same time. The resulting electrical and thermal efficiency of 45.3% and 43.6% we obtained were very similar to 45.2% and 43.4% in GE technical datasheet, respectively (GE Energy, 2009). It is well known that a gas engine would operate with less electrical efficiency if fed by a fuel gas having a lower heating value. As the syngas stream in this study has a LHV (lower heating value) of 187.4 kJ/mol (or 11.8 kJ/g) which is lower than 951.3 kJ/mol (or 49.0 kJ/g) of the natural gas, the estimated electrical efficiency was reduced to 41.9% while there was a slight increase of the thermal efficiency to 43.8% from 43.6%. In this study, it was assumed that the heat loss and the heat recovery at

the gas engine with the syngas feed would be the same as those at the gas engine with natural gas feed since the gas flowrates in the two cases were effectively the same. However, in a case where the gas mass flowrate is notably lower than those in the reference study and the base case, i.e. pre-combustion capture unit integration case, both heat loss and recovery were reduced in proportion to the ratio of the two gas mass flowrates. GE Energy (2010a) also reported the electrical and thermal efficiencies of 42.3% and 42.7%, respectively, in running the Jenbacher 620 gas engine with a wood gas originating from the FICFB biomass gasifier that this study is based on. The gas engine simulation with syngas feed was implemented making use of the UniSim simulation constructed for natural gas feed with the same adiabatic efficiencies of the devices that pressurise or depressurise fluid and with the same compression ratio of 11. The electrical and thermal efficiencies (41.9% and 43.8%) with syngas feed were close to those in the reference. The reduction in the power efficiency can be explained by the mean efficiency pressure of the gas engine decreasing with lower fuel gas LHV. For the gas engine with the syngas feed, the mean efficiency pressure was reduced to 17.8 bar while it was close to 20 bar for natural gas feed. In case 2 where the syngas is shifted and decarbonised, the mean efficiency pressure was increased to 18.6 bar due to the heating value being increased by decarbonisation. These comparisons vindicate that our gas engine model is good enough to be capable of estimating reasonably the change of electrical and thermal efficiencies with varying fuel gas LHV. This gas engine model will be used later for estimating the electrical and thermal efficiencies of the Jenbacher 620 gas engine running with a new fuel gas generated by treating the raw syngas with shift reaction followed by decarbonisation in case of a pre-combustion adsorptive carbon capture.

3. Case 1: Adsorption process for carbon capture

As mentioned in the introduction, an adsorption process would be advantageous over wet absorption processes for recovering CO_2 from a gas mixture having a higher CO_2 mole fraction at moderate scale industrial processes. Therefore, it was proposed to apply an adsorptive capture process rather than amine capture processes for capturing CO_2 from the syngas as shown in Fig. 2. As most CO_2-selective adsorbents exhibit very low CO adsorption amount, it is essential to convert most CO to CO_2 by water gas shift reaction (WGSR) for achieving a good carbon capture rate. A configuration of two-stage shift reactors in series made up of a high-temperature shift reactor followed by a low-temperature shift reactor was chosen to achieve 97.6% of overall CO conversion. The molar ratio of steam to CO in the feed to the 1st shift reactor was set as 2.0 (DOE NETL, 2010). Potentially the CO conversion could be increased by increasing the steam-to-CO ratio over 2.0 for the purpose of achieving higher CO_2 capture rate at the following adsorptive capture process. However the increase of steam-to-CO ratio requires greater consumption of thermal energy for producing more steam, leading to decreasing the thermal output. In addition, the resulting greater extent of exothermic CO conversion would reduce the total heat input to the gas engine being conveyed by shifted syngas leading to decreasing the power and thermal outputs at the gas engine. The gas composition of the shifted syngas after dehydration is 65.9% H_2, 32.6% CO_2, 0.6% CO, 0.8% N_2, and 0.1% CH_4 in molar percentage. For simplicity, it was assumed that N_2 and CH_4 would behave similarly to H_2 and CO, respectively, in the adsorption system so only three components of H_2, CO_2 and CO were considered as feed constituents.

A two-stage, two-bed PVSA unit was located downstream of the shift reactors for pre-combustion CO_2 capture as shown in Fig. 2. It has been reported that the two stages in series configurations could archive the CO_2 recovery as high as 90% and the CO_2 purities higher than 95% (Wang et al., 2013; Shen et al., 2012) when applied for post-combustion carbon capture. The cycle of each two-column PVSA stage was configured with either 4-step Skarstrom cycle or 6 step cycle incorporating pressure equalisation (PE) steps as shown in Fig. 3. The performances of the PVSA units made up of two non-adiabatic columns were simulated using the simulation parameters listed in Table 1 by an in-house adsorption process simulator (Friedrich et al., 2013; Luberti et al., 2014).

Table 1
Physical properties of zeolite 13X pellets, adsorption equilibrium and kinetic parameters and adsorption column parameters used in this study.

Physical properties	
Pellet density (ρ_p)	1200 kg/m^3
Pellet void fraction (ε_p)	0.25
Pellet average diameter (d_p)	4 mm
Pellet specific heat capacity (C_p)	920 J/kg K
Adsorption equilibrium and kinetic parameters	
Saturated adsorption capacity (q_s)	5.22 mol/kg
Mono-site Langmuir isotherm parameter $\left(b^o_{CO_2}\right)$	3.95×10^{-5} bar^{-1}
Mono-site Langmuir isotherm parameter $\left(b^o_{CO}\right)$	2.08×10^{-5} bar^{-1}
Heat of adsorption $\left(\Delta H_{CO_2}\right)$	32.6 kJ/mol
Heat of adsorption (ΔH_{CO})	20.3 kJ/mol
Linear driving force coefficient, $\left(k^{LDF,\ macro}_{CO_2}\right)$	75.1 s^{-1}
Linear driving force coefficient $\left(k^{LDF,\ macro}_{CO}\right)$	37.5 s^{-1}
Adsorption column parameters	
External bed void fraction (ε_b)	0.4
Axial mass dispersion coefficient (D^L)	1.80×10^{-4} m^2/s
Axial thermal dispersion coefficient (λ^L)	1.50 W/m K
Wall heat transfer coefficient (h_w)	80 W/m^2 K

3.1. Adsorbent

Zeolite 13X has been chosen as an adsorbent for the PVSA units in this work. Several researchers (Krishnamurthy et al., 2014; Xiao et al., 2008; Wang et al., 2013) have designed successfully PVSA cycles using zeolite 13X for carbon capture from the flue gases at PC-fired boiler power plants.

The physical properties of the zeolite 13X pellet and the associated equilibrium isotherm parameters were found in the paper (Hu et al., 2014) and they are listed in Table 1. Extended mono-site Langmuir isotherms were employed to predict the adsorption equilibria of CO_2 and CO on zeolite 13X. Due to the low H_2 partial pressure of around 1 bar, it was assumed that the H_2 would perform as an inert component. Also the effect of CO on the adsorption dynamics must be relatively small since the syngas feed contains only 0.6 mol% of CO after the high severity CO shift reaction. In this work, the equilibrium isotherms of N_2 and CO_2 on zeolite 13X were measured by Zero Length Column experiments in our lab and the two parameters of the extended mono-site Langmuir isotherms were estimated from the experimental data. It was assumed that the adsorption equilibrium isotherm of CO on zeolite 13X would be reasonably the same as that of N_2 on zeolite 13X since the N_2 isotherms we measured were very close to the reported CO isotherms (Saha and Deng, 2009) within the range of our PVSA process operation. Therefore, only three components, such as CO_2, CO and inert H_2, were taken into account in the adsorption simulation.

3.2. Simulation of two-stage PVSA units

The 1st stage PVSA is deemed as CO_2 enriching stage where the CO_2 molar percentage is increased to 60 to 75% with the CO_2 recovery maintained much higher than 90%. The following 2nd stage PVSA is regarded as CO_2 purification step for increasing the

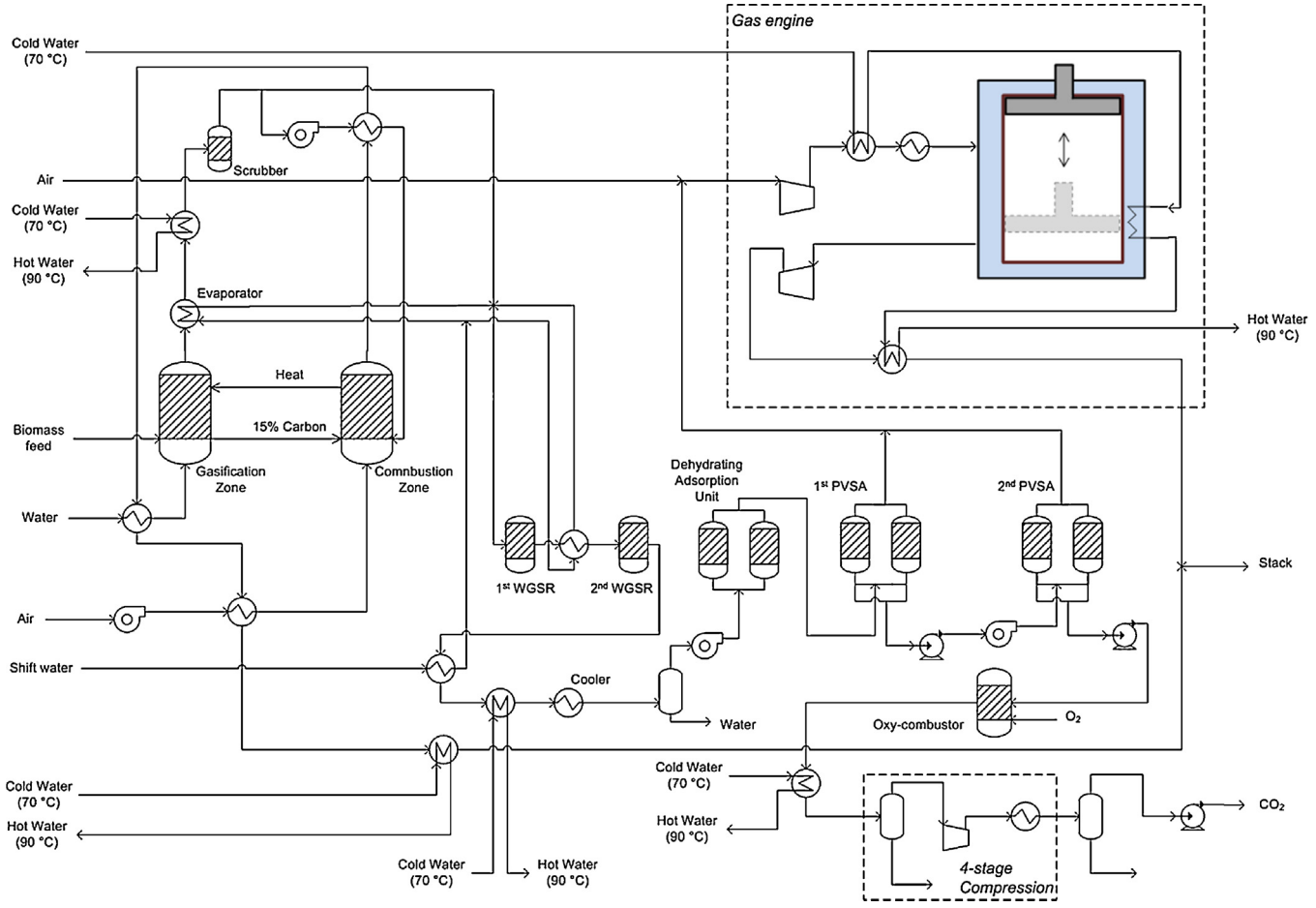

Fig. 2. Schematic diagram of a biomass gasification CHP plant integrated with a two-stage PVSA CO_2 capture unit (case 1).

CO_2 mole fraction over 95% at the sacrifice of the CO_2 recovery in order to achieve overall carbon (CO_2 + CO) recovery of around 87 to 88% that is equivalent to approximately 89 to 90% CO_2 recovery.

It is required to compress the feed gas up to 1.5 bar from 1.1 bar before being fed to each PVSA unit in order to create sufficient working capacity between adsorption and desorption. The optimal feed temperature must be higher than ambient temperature as pointed out by Xiao et al. (2008) for maximising the CO_2 working capacity given the CO_2 partial pressure difference between adsorption and desorption that is similar to those in this study. Therefore, the feed gas was cooled down to 57 °C after feed pressurisation at both stages of the PVSA units.

Table 2 shows the column dimension and the operating conditions of the two-stage PVSA units investigated in this study. The adsorption columns for the two-stage PVSA units were sized to have the length of 3 m for both of them and the internal radius of 1.20 to 1.22 m for the 1st PVSA and 0.99 to 1.18 m for the 2nd PVSA. The slight change of the internal radius over the runs is related to the superficial velocity at the column inlet during the adsorption step and the adsorption step time. For the 1st stage PVSA, the superficial velocity at the column inlet during adsorption step was kept constant for all the runs. Since the step times for column pressurisation and depressurisation were kept constant but the adsorption and purge step times were changed over the runs, the feed molar flowrate during adsorption step must be changed over the runs

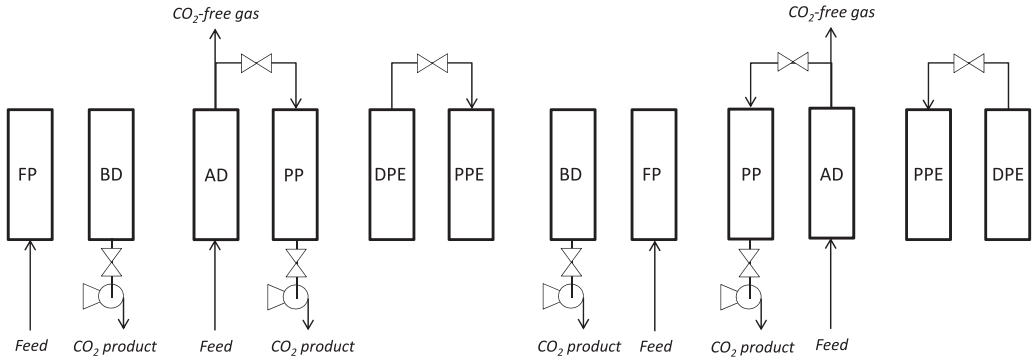

Fig. 3. Step configuration of a two-bed, six-step PVSA cycle (FP: feed pressurisation, AD: adsorption, DPE: depressurising pressure equalisation, BD: blowdown, PP: product purge, PPE: pressurising pressure equalisation).

Table 2
Operating conditions of two-stage PVSA units for carbon capture investigated in this study.

Run	1st stage PVSA unit							
	Desorption pressure [bar]	P/F ratio [%]	Column length [m]	Column radius [m]	Superficial velocity at adsorption step [Nm/s]	$t_{FP}/t_{AD}/t_{DPE}/t_{BD}/t_{PP}/t_{PPE}$ (t_{cycle}) [s]	CO_2 purity [%]	CO_2 Recovery [%]
Run 1	0.25	10	3	1.21	0.22	38.5/240/0/38.5/240/0 (557)	72.3	97.9
Run 2	0.30	10	3	1.21	0.22	38.5/240/0/38.5/240/0 (557)	72.6	95.7
Run 3	0.40	10	3	1.22	0.22	38.5/240/0/38.5/240/0 (557)	72.4	92.5
Run 4	0.40	17.5	3	1.20	0.22	38.5/300/0/38.5/300/0 (677)	63.3	97.1
Run 1_1PE	0.25	10	3	1.22	0.22	19.25/240/19.25/19.25/240/19.25 (557)	72.8	97.6
Run 1_2PE	0.25	10	3	1.22	0.22	19.25/240/19.25/19.25/240/19.25 (557)	72.8	97.6

Run	2nd stage PVSA unit								Overall PVSA	
	Desorption pressure [bar]	P/F ratio [%]	Column length [m]	Column radius [m]	Superficial velocity at adsorption step [Nm/s]	$t_{FP}/t_{AD}/t_{DPE}/t_{BD}/t_{PP}/t_{PPE}$ (t_{cycle}) [s]	CO_2 purity [%]	CO_2 Recovery [%]	CO_2 Recovery [%]	Carbon Recovery [%]
Run 1	0.40	0.46	3	0.99	0.14	53.5/214/0/53.5/214/0 (535)	95.0	91.8	89.8	87.8
Run 2	0.30	0.41	3	1.05	0.12	60/240/0/60/240/0 (600)	95.0	93.8	89.5	87.3
Run 3	0.20	0.41	3	1.18	0.09	75/300/0/75/300/0 (750)	95.2	96.8	89.3	87.4
Run 4	0.25	0.41	3	1.09	0.13	80/320/0/80/320/0 (800)	95.2	91.8	89.1	87.1
Run 1_1PE	0.40	0.46	3	1.00	0.13	53.5/214/0/53.5/214/0 (535)	95.1	91.2	88.9	87.0
Run 1_2PE	0.45	1.15	3	1.00	0.15	27/214/27/27/214/27 (536)	96.1	92.1	89.9	87.8

accordingly. Therefore, the superficial velocity was kept constant regardless of varying feed molar flowrates during adsorption step by changing the column radius. For the 2nd stage PVSA the superficial velocity during the adsorption step is highly correlated to the CO_2 recovery being achieved at the 1st stage PVSA. For example, the CO_2 recovery of the 1st stage PVSA in case 3 is so low in comparison to those in runs 1 and 2 that the loss of CO_2 at the 2nd stage must be reduced further to achieve the same overall CO_2 recovery. This can be done by reducing both the desorption pressure and the superficial velocity during the adsorption step at the 2nd stage. The drastic reduction in the superficial velocity allows us to use elongated adsorption step time in run 3. The higher column radius for the 2nd stage PVSA in case 4 can be explained with the higher feed flowrate at the 2nd stage caused by the lower CO_2 purity being achieved at the 1st stage PVSA.

Table 2 also reports purge pressures, purge-to-feed molar ratios (P/F ratios), step times for each PVSA configuration. In general it is expected that the CO_2 recovery would increase with lower desorption pressure, lower superficial velocity of the feed, shorter adsorption time and higher P/F ratio, all of which can prevent CO_2 in the feed from penetrating into the top end of the column during the adsorption step. This is because the CO_2 recovery is inversely proportional to the amount of CO_2 loss during the adsorption step. Meanwhile the CO_2 purity would be decreasing with abovementioned changes of operating conditions except for the desorption pressure.

By and large the power consumption of the PVSA unit highly depends on the choice of desorption pressure if the P/F ratio would be low enough for achieving a very high CO_2 purity or it changes only within a narrow range. Therefore it would be ideal to design a PVSA unit in such a way that the desorption pressure can be set as high as possible. However, increasing desorption pressure should be compensated by increasing P/F ratio, decreasing adsorption time, or decreasing superficial velocity in order to maintain the CO_2 recovery as high as possible. For the 1st stage PVSA, we can see clearly the expected trends that the CO_2 recovery decreases gradually with increasing desorption pressure from Run 1 to Run 3 through Run 2, i.e. 97.9% at 0.25 bar, 95.7% at 0.30 bar and 92.5% at 0.40 bar. It was thought that the CO_2 recovery of 92.5% in Run 3 would be a practical minimum to be achieved at the 1st stage PVSA for achieving the overall CO_2 recovery of 89%. The P/F ratio was increased from 10% to 17.5% in Run 4 in order to increase the CO_2 recovery back to around 97%. The increase of P/F ratio resulted in improving the CO_2 recovery so significantly that it could allow us to use a longer adsorption step time even with the same superficial velocity in Run 4.

Fig. 4 shows CO_2 mole fraction profiles along the column at the end of adsorption step for the 1st PVSA stage. As explained above, use of the higher desorption pressure in Run 3 deteriorates the CO_2 working capacity since the CO_2 could proceed to the column exit further during the adsorption step. The lower CO_2 recovery can be explained by the higher CO_2 mole fraction at the column end, indicating greater CO_2 loss during the adsorption step. In case of Run 4 against Run 3, the increasing P/F ratio could recover the CO_2 working capacity greatly and accordingly the CO_2 profile was held further back from the column exit.

The effect of including pressure equalisation steps into the cycle was also investigated. Incorporating the PE steps into the PVSA cycle are expected to increase the CO_2 purity since light components existing more abundantly near the top end of the column than near the bottom end would be transferred to the top end of the other column during the PE steps. On the contrary, it is likely that the CO_2 recovery would be slightly decreased since the CO_2 contained in the gas flow during the PE steps is transferred to the top end of the associated pressurising column and then it is easy to be lost during the following adsorption step. It was observed that, in comparison to Run 1, the Run 1_1PE and 1_2PE incorporating the PE steps could increase the CO_2 purity but resulted in decreasing the CO_2 recovery a little bit.

The pre-treated CO_2 product obtained during the blowdown and purge steps of the 1st stage PVSA was used as a feed of the subsequent 2nd stage PVSA simulation. Depending on the CO_2 purity and recovery at the 1st stage PVSA, the operating conditions of the 2nd stage PVSA need to be adjusted in order to achieve the targets of CO_2 purity and recovery. In case of Run 1, a relatively high desorption pressure of 0.40 bar was permitted to achieve the targets since very high CO_2 purity and recovery were already obtained at the associated 1st stage PVSA. However, with the CO_2 recoveries at the 1st stage PVSA decreasing from 97.9% to 92.5% over the Runs 1 to 3, the required desorption pressure was required to decrease gradually up to 0.20 at Run 3 to obtain the higher CO_2 recovery at the 2nd stage PVSA. At the same time the superficial velocity was reduced

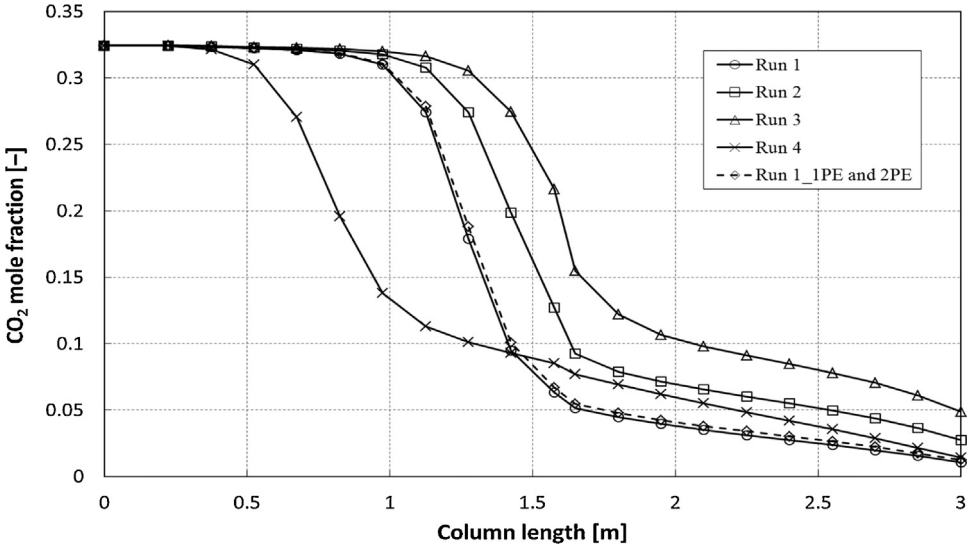

Fig. 4. CO_2 mole fraction profile along the column at the end of adsorption step of the 1st stage PVSA unit.

to increase the CO_2 recovery. Since decreasing superficial velocity could make the adsorption column dynamics more equilibrium-controlled, use of longer adsorption step times was allowed. In Run 4 requiring the greatest improvement of the CO_2 purity at the 2nd stage, the CO_2 purity improvement was made by using the longest adsorption step. As shown in Fig. 5, the CO_2 profile in Run 4 was allowed to approach the column exit further than those in Runs 2 and 3 in order to achieve the greatest CO_2 purity improvement at the 2nd stage.

A 4-step Skarstrom cycle was used for the 2nd stage PVSA of Run 1_1PE while a 6-step cycle including PE steps was applied to the 2nd stage PVSA of Run 1_2PE. The resulting CO_2 purity and recovery at the 2nd stage of Run 1_1PE are very similar to those of Run 1 since the feed gas and the operating conditions of the two cases are almost identical. On the contrary, it is very interesting to observe that the Run 1_2PE achieved the targets with higher desorption pressure and higher P/F ratio than those of the Run 1_1PE. This is because adding the PE steps increases the CO_2 purity to such a great extent that it can allow us to use higher P/F ratio. Several simulations were carried out to achieve the CO_2 purity and recovery targets in case of Run 1_2PE prior to finding the optimum operating conditions as shown in Table 2. First, 0.40 bar of desorption pressure and 0.46% of P/F ratio that are the same as those of Run 1_1PE resulted in 96.5% of CO_2 purity and 90.7% of CO_2 recovery. It indicated that the use of PE steps contributed to increasing the CO_2 purity at the sacrifice of CO_2 recovery. Since the CO_2 purity is sufficiently higher than the target while the CO_2 recovery is too low for the target, the P/F ratio was increased from 0.46% to 1.15% in the second trial. The P/F ratio increase reduced the CO_2 purity down to 95.8% but increased the CO_2 recovery up to 94.1%. As the CO_2 recovery is higher than the target at the second trial, the desorption pressure was increased up to 0.45 bar in the third trial. In the third trial, the CO_2 purity and recovery are close to the targets as shown in Table 2. Since the CO_2 purity is still higher than 95%, however, it may allow higher desorption pressure and higher P/F ratio to achieve the targets, leading to further decrease in the power consumption.

Table 3 shows the power consumptions for feed pressurisation using a blower and for evacuation using a vacuum pump during blowdown and product purge steps. The power consumptions were estimated by

$$P_{\text{Blower}} = \frac{1}{\eta_{\text{Blower}}} \text{FM} \left(\frac{\gamma}{\gamma - 1}\right) \left(\frac{1.1\,\text{bar}}{\rho_{\text{in}}}\right) \left[\left(\frac{1.5\,\text{bar}}{1.1\text{bar}}\right)^{((\gamma-1)/\gamma)} - 1\right] \quad (1)$$

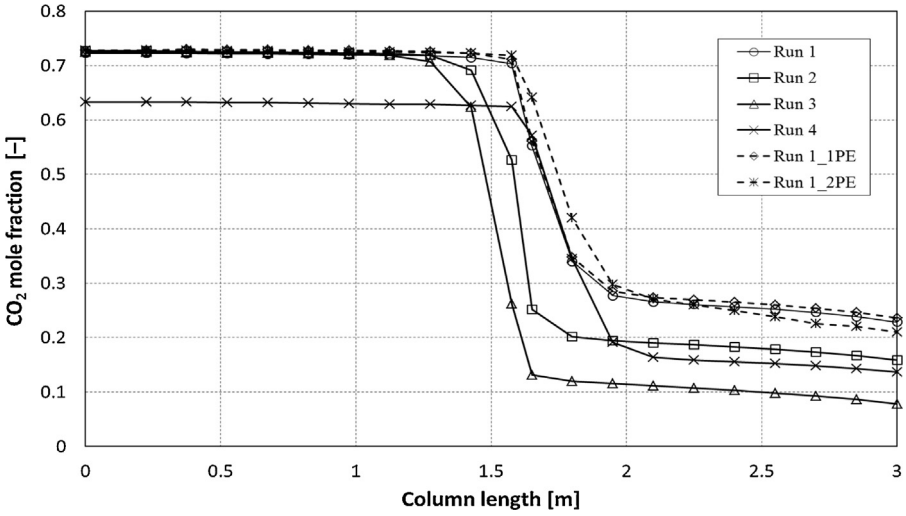

Fig. 5. CO_2 mole fraction profile along the column at the end of adsorption step of the 2nd stage PVSA unit.

Table 3
Power consumptions of various two-stage PVSA units for carbon capture [unit: kW_e].

Runs	1st stage PVSA unit			2nd stage PVSA unit			Overall	
	Feed pressurisation (1.1 → 1.5 bar)	Evacuation (P_{des} → 1.1 bar)	Sub-total	Feed pressurisation (1.1 → 1.5 bar)	Evacuation (P_{des} → 1.1 bar)	Sub-total	Total	Specific power consumption [MJ_e/kg of CO_2]
Run 1	39.6	90.7	130.3	17.2	41.7	58.8	189.1	0.367
Run 2	39.6	76.8	116.4	16.8	54.6	71.4	187.9	0.366
Run 3	39.6	56.1	95.7	16.3	74.2	90.5	186.2	0.363
Run 4	39.6	67.4	107.0	19.6	62.6	82.2	189.2	0.370
Run 1_1PE	39.6	90.2	129.8	17.1	41.2	58.3	188.0	0.369
Run 1_2PE	39.6	90.2	129.8	17.1	36.2	53.2	183.0	0.355

$$P_{\text{Vacuum pump}} = \frac{1}{\eta_{\text{Vacuum pump}}} \text{F M} \left(\frac{\gamma}{\gamma - 1}\right) \left(\frac{P_{\text{des}}}{\rho_{\text{in}}}\right) \times \left[\left(\frac{1.1\,\text{bar}}{P_{\text{des}}}\right)^{((\gamma-1)/\gamma)} - 1\right] \quad (2)$$

It should be noted that P_{des} in Eq. (2) is the desorption pressure in Table 2 that was set for each run and the desorption pressure instead of decreasing internal column pressure must be used for the blowdown step as well as the purge step. This is because the desorption pressure was used as a boundary condition of a valve equation to determine the time-dependant column pressure during the blowdown step.

As shown in Table 3, it can be observed that the power consumption for evacuation depends mostly on the desorption pressure but it is also affected by the P/F ratio to a lesser extent. Surprisingly, the overall power consumptions over the runs are almost identical as 188 to 189 kW except for the Run 1_2PE, indicating that if the 1st stage was designed at higher desorption pressure or less P/F ratio, the power saving effect made at the 1st stage PVSA would be counterbalanced by greater power consumption at the associated 2nd stage PVSA requiring lower desorption pressure or higher P/F ratio. As mentioned above, incorporating PE steps into the 2nd stage PVSA could increase the CO_2 purity greatly so it allows us to use the higher P/F ratio without reducing the CO_2 recovery under the target even with the higher desorption pressure.

3.3. Downstream processes

In this study the overall biomass gasification CHP plant integrated with the two-stage PVSA unit was simulated on the basis of separation performance at Run 1. The slip of small H_2 and trace amounts of CO, CH_4 and N_2 into the CO_2 product cannot be avoided as a result of operating the PVSA unit. The H_2, CO and trace CH_4 contained in the CO_2 product should be removed before the CO_2 product is sent to the CO_2 compression unit.

In case of Run 1, the CO_2 product being produced at the 2nd stage PVSA unit contains 4.8% H_2 and 0.2% CO. To convert the H_2 and CO into CO_2, an oxy-combustor was installed downstream of the 2-stage PVSA unit as shown in Fig. 2. In this study, it was assumed that the pure oxygen required for operating the oxy-combustor would be sourced by purchasing it from external suppliers rather than deploying and operating a dedicated distillation-based Air separation unit (ASU) to produce pure oxygen in situ given the fact that the required oxygen flowrate is only 0.01 kg/s. It was reported that the power consumption involved in the ASU operation is around 231 kW h/t of O_2 (Ozcan et al., 2013). The power consumption must be taken into account as energy penalty in the case 1 using adsorptive carbon capture. Additional hot water production is available by recovering the heat from the oxy-combustor flue gas. The resulting CO_2 purity was increased up to over 99.9% after water being condensed out.

The shift reaction for pre-treating the syngas decreases the LHV of the fuel gas due to its exothermic reaction. However, as the subsequent two-stage PVSA unit removes the CO_2 out of the shifted syngas, the heating value of the resulting syngas increases. As a result the LHV of fuel gas is estimated to be 228.9 kJ/mol that is greater than 187.4 kJ/mol of the raw syngas. The electrical efficiency of the gas engine on the basis of syngas was slightly increased by 1.2% point due to the increase of the fuel gas LHV (see Table 4).

Once the CO_2 product is produced by the two-stage PVSA unit, it is compressed by a multi-stage CO_2 compression system consisting of four-stage CO_2 compressors followed by one CO_2 pump up to 153 bar from 1.1 bar.

4. Case 2: Amine process for carbon capture

A conventional amine capture process using 30 wt% aqueous MEA was attached to a gas stream combining the two flue gases from the gas engine and the gasifier combustor as shown in Fig. 6. The amine process was designed for achieving 90% CO_2 capture from the biomass gasification CHP plant. The process configuration and the operating conditions of the conventional amine process were explained in our earlier work (Ahn et al., 2013). It is well known that the required heat duty at the stripper reboiler can be reduced to around 3.5 MJ_{th}/kg CO_2 when the amine process is optimised where the stripper pressure on its top is set as 1.9 bar. Therefore, the amine process can generate the CO_2 product at 1.9 bar that is higher than 1.1 bar of the CO_2 product pressure at the PVSA units. As a result, the specific power consumption for compressing the CO_2 product up to 153 bar must be lower at the amine process than those at the PVSA units.

In addition to the heat duty of 3.5 MJ_{th}/kg CO_2 at the stripper reboiler, the amine process also consumes power for operating a feed gas blower and several solvent pumps. The thermal and power consumptions for amine process are listed in Table 4.

In contrast to the PVSA system consuming only power, an amine process requires both heat and power for the operation but most of the energy it consumes is the thermal energy for the reboiler operating with LP steam. While PC-fired power plants or combined cycle power plants already have steam cycles where a LP steam for the stripper reboiler is available by steam extraction from the IP/LP crossover, the biomass gasification CHP plant does not have any steam cycle, so no stream is available for the stripper reboiler on site. Therefore, the LP steam should be generated separately in case of retrofitting an amine process into the biomass gasification CHP plant.

There are two options to generate a LP steam for the stripper reboiler: the first option is to recover the heat from the biomass gasification CHP plant for generating the required amount of LP steam by reducing hot water production. In other words, a CO_2-laden solvent is regenerated at a steam stripper being driven by in-situ generated LP steam. Theoretically, this option is possible since the required heat duty for 90% CO_2 recovery at an amine process amounting to 3.34 MW_{th} (see Table 4) is sufficiently lower

Table 4
Summary of the performances of biomass-fuelled CHP plants without and with carbon capture.

	Base case	Case 1: WGSR + PVSA	Case 2: biomass-fired boiler CHP + MEA
Biomass-fueled CHP plant			
Biomass heat input, LHV [MW_{th}]	10.07	10.07	10.07 (+4.49)
Syngas LHV [kJ/mol]	187.4	228.9 (shifted)	187.4
Syngas heat flow, LHV [MW_{th}]	6.91	6.37	6.91
Gas engine performance			
Electricity production [MW_e]	2.89	2.74	2.89
Power efficiency on the basis of biomass/syngas	28.7%/41.9%	27.2%/43.1%	28.7%/41.9%
Hot water production [MW_{th}]	3.03	2.80	3.03
Thermal efficiency on the basis of biomass/syngas	30.1%/43.8%	27.8%/43.9%	30.1%/43.8%
Hot water generation at gasification section [MW_{th}]	2.09	1.71	2.09
Power consumption at gasification section [MW_e]	0.09	0.09	0.09
Biomass-fired boiler CHP plant for steam generation			
Biomass heat input, LHV [MW_{th}]	–	–	4.49
Power generation at steam turbine [MW_e]	–	–	0.643
Steam pressure and temperature at the turbine inlet	–	–	28 bar, 370 °C
LP steam generation for amine process [MW_{th}]	–	–	3.34
Hot water generation [MW_{th}]			0.031
Heat-to-power conversion factor, –	–	–	0.162
Power consumption [MW_e]	–	–	0.021
Net power generation [MW_e] (efficiency)	–	–	0.622 (13.9%)
Net thermal generation [MW_{th}] (efficiency)	–	–	3.37 (75.1%)
Carbon capture unit			
Process		WGSR + PVSA + oxy-combustor	MEA
Power consumption [MW_e]	–	0.189	0.100
Heat consumption [MW_{th}]	–	–	3.34
Power consumption, CO_2 compression [MW_e]	–	0.166	0.261
Power consumption for oxygen production [MW_e]	–	0.008	–
Hot water generation at oxygen combustor [MW_{th}]	–	0.178	–
Hot water generation at WGSR [MW_{th}]		0.167	–
Carbon capture rate on biomass basis [%]	–	48.5% (87.3% on the syngas basis)	58.4% (90.0% on the biomass-gasification CHP plant flue gas basis)
Specific power consumption per CO_2 captured (including CO_2 compression) [MJ_e/kg CO_2]	–	0.986 (0.698, excluding the effect of power generation reduction at gas engine)	1.02
Specific thermal consumption per CO_2 captured [MJ_{th}/kg CO_2]	–	0.510	2.32
Overall performance			
Net power generation [MW_e] (efficiency)	2.80 (27.8%)	2.29 (22.7%)	3.06 (21.0%)
Net hot water generation [MW_{th}] (efficiency)	5.12 (50.8%)	4.86 (48.2%)	5.15 (35.4%)
Sum of the net power and thermal efficiencies	78.6%	70.8%	56.4%

than the total heat production of 5.12 MW_{th} that the biomass gasification CHP plant can generate as hot water (Oreggioni et al., 2014). However, the required heat duty is so huge that the heat recovery at the gasification section only is not large enough to generate the entire amount of LP steam required for the amine process. Therefore it is necessary to modify part of the gas engine configuration relating to hot water production as well as the gasification section for producing the required LP steam.

As a result it is inevitable that the net overall thermal efficiency would be greatly reduced. Strictly speaking the biomass CHP plant being integrated with the amine process in this way cannot be regarded as a CHP plant any more even though it could achieve 90% carbon capture at case 2 in comparison to 48.5% at case 1. If the carbon capture rate at case 2 were reduced roughly by half so that it could be close to the carbon capture rate at case 1, the CHP plant might be able to produce a decent amount of heat as well as power. However, it is not plausible that any CHP plant operator would build an amine process in a scale to achieve only 48.5% carbon capture rate instead of 90% since the reduction of the investment cost being expected by reducing the capacity of the amine process would not be great.

The second option is to install a new biomass-fired boiler CHP plant inherently having a much higher thermal efficiency (75.1%) than those of the biomass gasification CHP plant (50.8%) in order to produce the heat required for the amine process capturing 90% CO_2 only from the flue gas of the biomass gasification CHP plant as shown in Fig. 6. The second option has a clear advantage over the first option in that there is no need to modify the original biomass gasification CHP plant for LP steam generation and the net power and thermal generation can be maintained over the non-capture case by feeding more biomass to the system.

In the new biomass-fired boiler CHP plant, an additional biomass feed, amounting to around 45% of the biomass used in the base case, enters the boiler where it is combusted with air to generate the superheated steam of 370 °C and 28 bar. The superheated steam is used for power generation with a single steam turbine and subsequently the exhaust steam needs to be conditioned to 134 °C and 3 bar at a heat exchanger in order to make the steam suitable for its direct supply to the stripper reboiler. At the heat exchanger for steam conditioning, a little bit of hot water can be produced in addition. Once the LP steam is condensed at the stripper reboiler, the condensed water is recycled to the deaerator (not shown in Fig. 6). Then the deaerated BFW is pressurised by a BFW pump and subsequently sent to the boiler to complete the steam cycle.

5. Performance analysis of two CO_2 capture cases

The performances of the base case and the two carbon capture cases are summarised in Table 4. To quantify the energy penalties involved in the CHP plant retrofits, two different indices were proposed in this study reflecting the characteristics of the CHP plant; the specific power consumption per captured CO_2 and the specific thermal consumption per captured CO_2. This is because, given the process configuration of the biomass gasification CHP plant, the power and heat being generated are independent of each other, that is to say, the amount of power generation by a gas engine is not affected by that of heat production by means of heat recovery. In other words, power and heat are not interchangeable with each

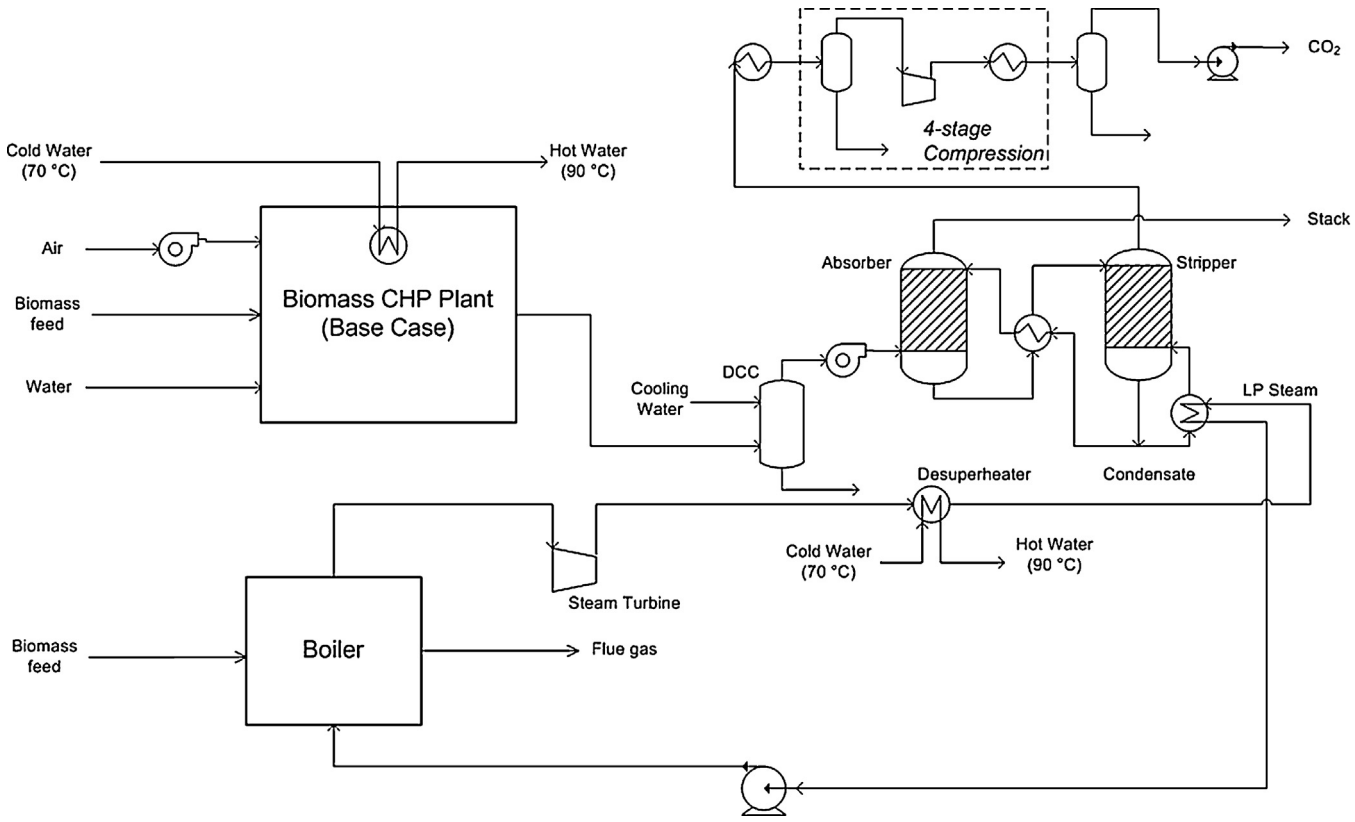

Fig. 6. Schematic diagram of a biomass gasification CHP plant integrated with an amine CO_2 capture unit (case 2).

other in a biomass gasification CHP plant. In the marked contrast to the CHP plants, a power plant with steam cycle can be evaluated with a unified, single specific power (or heat) consumption per captured CO_2 to quantify the energy penalty involved in carbon capture integration (Ahn et al., 2013).

The specific power consumption of unit CO_2 captured (MJ_e/kg) is calculated by

$$\text{Specific power consumption}_{\text{case 1(adsorption)}} = \frac{P_{c,\ \text{PVSA}} + P_{c,\ \text{CO}_2\ \text{compression}} + P_{c,\ \text{O}_2\ \text{production}} + \left(P_{g,\ \text{engine\_base}} - P_{g,\ \text{engine\_case 1}}\right)}{F_{\text{captured CO}_2}} \quad (3)$$

$$\text{Specific power consumption}_{\text{case 2(Amine)}} = \frac{P_{c,\ \text{amine}} + P_{c,\ \text{CO}_2\ \text{compression}} + Q_{\text{boiler CHP}} \times \eta_{e,\ \text{gasification CHP}} - P_{g,\ \text{boiler CHP}}}{F_{\text{captured CO}_2}} \quad (4)$$

The specific thermal consumption of unit CO_2 captured (MJ_{th}/kg) is estimated by

$$\text{Specific thermal consumption}_{\text{case 1(adsorption)}} = \frac{\left(H_{g,\ \text{engine\_base}} - H_{g,\ \text{engine\_case 1}}\right) + \left(H_{g,\text{gasification\_base}} - H_{g,\text{gasification\_case 1}}\right) - H_{g,\text{WGSR}} - H_{g,\text{oxycombustor}}}{F_{\text{captured CO}_2}} \quad (5)$$

$$\text{Specific thermal consumption}_{\text{case 2(Amine)}} = \frac{Q_{\text{boiler CHP}} \times \eta_{\text{th,\ gasification CHP}} - H_{g,\ \text{boiler CHP}}}{F_{\text{captured CO}_2}} \quad (6)$$

As shown in Table 4, the specific power consumptions in both cases are very similar to each other even though the amine process requires much less power consumption than the adsorption process does. This can be explained by the very low power efficiency of the new biomass-fired boiler CHP plant in case 2. The additional biomass feed for the new biomass-fired CHP plant would be used for a biomass gasification CHP plant with higher power efficiency if no carbon capture was required. Therefore, the difference between the expected power generation at the biomass gasification CHP with the additional biomass feed for the new biomass-fired boiler CHP, denoted by $Q_{\text{boiler CHP}} \times \eta_{e,\text{ gasification CHP}}$, and the actual power generation at the new biomass-fired boiler CHP, $P_{g,\text{ boiler CHP}}$, must be considered as an energy penalty in addition to the actual power consumption at the amine process itself.

It should be highlighted that the specific power consumption in case 1 must take into account the effect of exothermic shift reaction as well as power consumption at the carbon capture PVSA unit. Without including the effect of shift reaction, the specific power consumption would be reduced to be as low as 0.698 MJ_e/kg CO_2. However, due to the exothermic reaction taking place in the shift reactors, the total heat input to the gas engine by feeding the shifted syngas was greatly reduced. As a result, the power generation at the gas engine was decreased accordingly as shown in Table 4. The

difference of power generations at the gas engine between base case and case 1 must be considered as an energy penalty.

A similar approach was taken for estimating the specific thermal consumption per captured CO_2. The additional biomass feed for the new boiler CHP plant would be used for a biomass gasification CHP plant without having to implement carbon capture. Since the thermal generation in the existing gasification CHP plant does not change in case 2 due to the LP steam for the amine process being entirely sourced from the new boiler CHP plant, the energy penalty can be estimated by the expected thermal production at the gasification CHP plant with the heat input by additional biomass feed to the new CHP plant, $Q_{\text{boiler CHP}} \times \eta_{\text{th,gasification CHP}}$. It should be noted in Table 4 that the specific thermal consumption in case 2 (2.32 MJ_{th}/kg CO_2) was less than the 3.5 MJ_{th}/kg CO_2 of the actual specific thermal consumption. This is because some of the thermal consumption was considered as the specific power consumption in this approach due to the difference of the net power and thermal efficiencies between the two biomass-fuelled CHP plants.

Comparing the resulting net energy efficiencies between cases 1 and 2, the net thermal efficiency was 12.8% points higher at case 1 than at case 2 while the net power efficiency at case 1 was slightly higher by 1.7% points than that at case 2. This comparison clearly exhibits that the adsorption capture process would be more economical than the amine process for carbon capture from a biomass-gasification CHP plant.

6. Conclusions

In this study, a two-stage PVSA process was designed and simulated for carbon capture from a syngas stream at a biomass gasification CHP plant. To rigorously evaluate the energy penalty involved in the adsorption capture unit, process simulation for exemplary 10 MW_{th} biomass gasification CHP plant integrated with the PVSA unit was implemented. The change of the heat and power generation at the gas engine was also reasonably estimated using the UniSim simulation when the fuel gas was changed from the raw syngas to the decarbonised shifted gas.

The case study of carbon capture using adsorption was compared with another case of carbon capture using conventional amine capture unit in order to evaluate its performance in terms of the specific electrical and thermal consumptions involved in carbon capture and the overall heat and power efficiencies to be achieved. It was successfully demonstrated by process simulation that adsorptive capture unit could be more economical than conventional amine capture unit in all aspects.

However, it should be noted that there is a constraint on the maximum carbon capture rate achievable with the pre-combustion adsorptive carbon capture proposed in this study because the CO_2 emitted from the gasification combustor cannot be captured with the current process design.

To overcome this constraint, a follow-up study is underway to enhance the overall carbon capture rate up to greater than 49%. In the improved process being developed, the CO_2 involved in the combustion zone can easily be captured by feeding pure oxygen instead of air as the oxidant. The pure oxygen required for oxy-combustion at combustion zone as well as the oxy-combustor for post-treating the CO_2 product can be produced in situ by deploying a small-scale oxygen production Pressure Swing Adsorption unit.

Acknowledgements

We would like to express our gratitude for the financial support from EPSRC (grants no.: EP/F034520/1, EP/J018198/1, EP/J02077X/1 and EP/J020788/1) and KETEP (grant no.: 2011-8510020030).

Appendix A. Supplementary data

Supplementary data associated with this article can be found, in the online version, at doi:10.1016/j.ijggc.2015.01.008.

References

Ahn, H., Luberti, M., Liu, Z., Brandani, S., 2013. Process configuration studies of the amine capture process for coal-fired power plants. Int. J. Greenhouse Gas Control 16, 29–40.

Bridgewater, A.V., 1995. The technical and economic feasibility of biomass gasification for power generation. Fuel 74 (5), 631–653.

DOE NETL, 2010. Cost and Performance Baseline for Fossil Energy Plants Volume 1: Bituminous Coal and Natural Gas to Electricity Rev. 2, Pittsburgh, PA, US.

Francois, J., Abdelouahed, L., Mauviel, G., Patisson, F., Mirgaux, O., Rogaume, C., Rogaume, Y., Feidt, M., Dufour, A., 2013. Detailed process modeling of a wood gasification combined heat and power plant. Biomass Bioenergy 51, 68–82.

Friedrich, D., Ferrari, M.-C., Brandani, S., 2013. Efficient simulation and acceleration of convergence for a dual piston pressure swing adsorption system. Ind. Eng. Chem. Res. 52 (26), 8897–8905.

Hofbauer, H., Veronik, G., Fleck, T., Rauch, R., Mackinger, H., Fercher, E., 1997. The FICFB-gasification process. In: Developments in Thermochemical Biomass Conversion., pp. 1016–1025, http://members.aon.at/biomasse/banff.pdf

Hu, X., Mangano, E., Friedrich, D., Ahn, H., Brandani, S., 2014. Diffusion mechanism of CO_2 in 13X zeolite beads. Adsorption 20, 121–135.

GE Energy, 2009. Cogeneration Application Considerations. GE Energy, ⟨http://site.ge-energy.com/prod_serv/products/tech_docs/en/downloads/GER3430G.pdf⟩ as of 12/01/15.

GE Energy, 2010a. Jenbacher Type 6. GE Energy, ⟨http://site.ge-energy.com/prod_serv/products/recip_engines/en/downloads/ETS_E_T6_10_screen_August2010.pdf⟩ as of 12/01/15.

GE Energy, 2010b. Jenbacher Gas Engines a Variety of Efficient Applications. GE Energy, ⟨http://teb.com.ro/teb/upl/pdf/ev-prez2.pdf⟩ as of 12/01/15.

IPCC, 2005. Carbon Dioxide Capture and Storage. IPCC, Cambridge University Press, Geneva, Switzerland.

IPCC, 2014. Fifth Assessment Report. IPCC, Cambridge University Press, Geneva, Switzerland.

Krishnamurthy, S., Rao, V.R., Guntuka, S., Sharratt, P., Haghpanah, R., Rajendran, A., Amanullah, M., Karimi, I.A., Farooq, S., 2014. CO_2 capture from dry flue gas by vacuum swing adsorption: a pilot plant study. AIChE J. 60 (5), 1830–1842.

Luberti, M., Friedrich, D., Brandani, S., Ahn, H., 2014. Design of a H_2 PSA for cogeneration of ultrapure hydrogen and power at an advanced integrated gasification combined cycle with pre-combustion capture. Adsorption 20, 511–524.

Obernberger, I., Thek, G., 2008. Cost assessment of selected decentralised CHP applications based on biomass combustion and biomass gasification. In: Proceedings of the 16th European Biomass Conference & Exhibition.

Oreggioni, G.D., Friedrich, D., Brandani, S., Ahn, H., 2014. Techno-economic study of adsorption processes for pre-combustion carbon capture at a biomass CHP plant. Energy Procedia 63, 6738–6744.

Ozcan, D.C., Ahn, H., Brandani, S., 2013. Process integration of a Ca-looping carbon capture process in a cement plant. Int. J. Greenhouse Gas Control 19, 530–540.

Ruthven, D.M., 1984. Principles of Adsorption and Adsorption Processes. John Wiley & Sons, New York, US.

Saha, D., Deng, S., 2009. Adsorption equilibria and kinetics of carbon monoxide on zeolite 5A, 13×, MOF-5, and MOF-177. J. Chem. Eng. Data 54, 2245–2250.

Sartor, K., Quoilin, S., Dewallef, P., 2014. Simulation and optimization of a CHP biomass plant and district heating network. Appl. Energy 130, 474–483.

Schuster, G., Loffler, G., Weigl, K., Hofbauer, H., 2001. Biomass steam gasification—an extensive parametric modeling study. Bioresour. Technol. 77 (1), 71–79.

Shen, C., Liu, Z., Li, P., Yu, J., 2012. Two-stage VPSA process for CO_2 capture from flue gas using activated carbon beads. Ind. Eng. Chem. Res. 51 (13), 5011–5021.

Simader, G.R., 2004. Case study: 2MWel biomass gasification plant in Gussing (Austria). In: European Commission (Directorate-General for Energy and Transport).

US EPA, 2007. Biomass Combined Heat and Power Catalog of Technologies. US EPA.

Wang, L., Yang, Y., Shen, W., Kong, X., Li, P., Yu, J., Rodrigues, A.E., 2013. CO_2 capture from flue gas in an existing coal-fired power plant by two successive pilot-scale VPSA Units. Ind. Eng. Chem. Res. 52 (23), 7947–7955.

Xiao, P., Zhang, J., Webley, P., Li, G., Singh, R., Todd, R., 2008. Capture of CO_2 from flue gas streams with zeolite 13X by vacuum-pressure swing adsorption. Adsorption 14, 575–582.

Yang, R.T., 1997. Gas Separation by Adsorption Processes. Imperial College Press, Imperial College Press, London, UK.